Rocznik Ochrona Środowiska

Volume 26 Year 2024 ISSN 2720-7501 pp. 01-17

https://doi.org/10.54740/ros.2024.001 open access

Received: January 2024 Accepted: January 2024 Published: January 2024

Selected Agricultural Analyses Based on Data from MultiSen-PL, the Multi-sensor Airborne Remote Sensing Station

Marta Sieczkiewicz[1], Łukasz Jedynak[1], Ireneusz Wyczałek[1,2], Michał Wyczałek-Jagiełło[1]*

[1]GISPRO SA, Szczecin, Poland

[2]Faculty of Civil and Environmental Engineering and Architecture, Bydgoszcz University of Science and Technology, Poland

https://orcid.org/0000-0003-3963-8186

[*]corresponding author's e-mail: marta.sieczkiewicz@gispro.pl

Abstract: The RE band of electromagnetic radiation has recently become the subject of interest in remote sensing due to its greater penetration into the plant structure than the commonly used NIR band. It is particularly important in cultivating corn, which is characterised by considerable thick foliage during the growth period. While sensors equipped with this channel are used in satellite remote sensing and onboard drones, they are not implemented in airborne imaging systems. An airborne remote sensing station was constructed, including, in addition to the traditional R, G, B and NIR image components, also the RE channel and a laser scanner (ALS). Data processing involves geometric calibration and the creation of a multi-channel orthophoto map. The data processed in this way was tested by analysing several series of aerial recordings of a corn field, which involved developing interpretation keys based on selected vegetation indices and assigning individual groups of pixels with five plant health classes. This study focused on the comparative assessment of the effects of using the NDVI, GNDVI, NDRE and SAVI indices, comparing their results to yield measurements (CHM) and the results of field measurements of plants at the end of the growing season. Promising results with a high degree of correlation were obtained.

Keywords: remote sensing station, agricultural analyses, RE band, Vegetation Indices

1. Introduction

1.1. Agricultural context of remote sensing applications

The subject of advancing the exact cultivation of crops has been a recent focal point in various publications. These studies are directed towards either updating cultivation methods, promoting environmental conservation, or devising specific technical support approaches for agriculture. Ongoing research includes efforts to automate data acquisition and processing for intelligent decision-making systems like SDSS (Tian-en et al. 2009). A successful and dependable decision-making process in precision agriculture necessitates accurate, up-to-date, comprehensive, and detailed data. Such data forms the foundation for accurate conclusions drawn by analytical systems.

Data sources utilised in agricultural support procedures encompass soil and crop monitoring techniques relying on satellite, aerial, or ground remote sensing systems (Mulla 2013, Martinelli et al. 2015, Mogili et al. 2018, Triantafyllou et al. 2019). Ongoing developments include imaging in various bands of electromagnetic radiation alongside parameters such as humidity, evapotranspiration, temperature, and the chemical composition of both soil and plants (Camilli et al. 2007, Bogue 2017). To facilitate these endeavours, weather stations and various specialised sensors used in agriculture are employed (Fisher & Kebede 2010, Diedrichs et al. 2014). The GNSS satellite technique serves as a common positioning method, while GIS is a tool for mapping and spatial analysis (Tian-en et al. 2009, Tayari et al. 2015). The outcome of spatial data development typically results in a thematic map illustrating the existing situation (diagnostics) or recommending actions based on analysis, synthesis, and decision support methods (Camilli et al. 2007, Vogels 2017). Artificial intelligence (AI) is increasingly harnessed to support analysis and reasoning (Rose & Chilvers 2018).

In every agricultural application, the monitoring system is designed to furnish relevant data, which must subsequently undergo processing, including at least preliminary corrections and transformations to facilitate the indexing or classification process. The outcome of these actions is to depict the current state in the form of a map and/or specify recommended agrotechnical measures. It includes identifying the appropriate fertilisers or protective products to be used and their quantities in specific locations. Figure 1 illustrates this process, based on integrated agronomic and remote sensing data, as presented in (Radočaj et al. 2022) for precision agriculture applications.

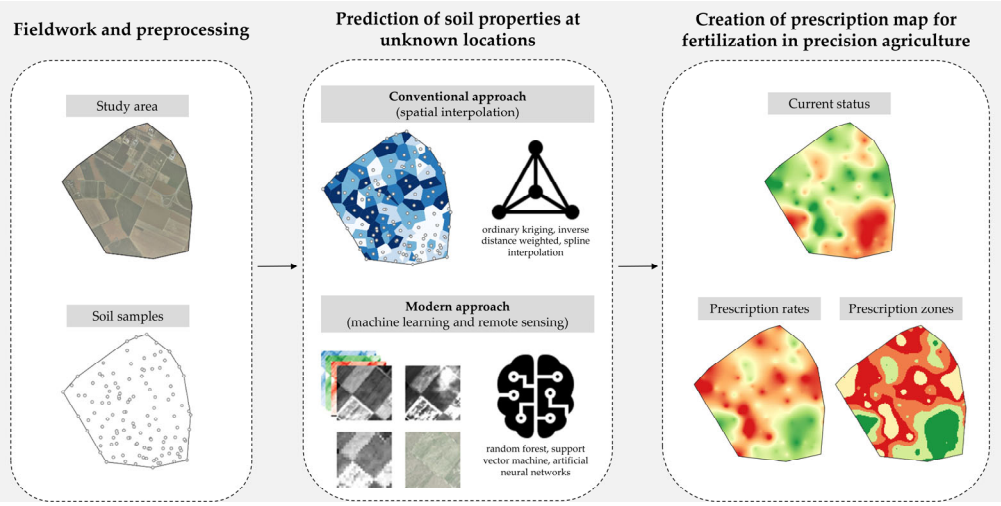

Fig. 1. The three steps suggested by Radočaj et al. (2022) for determining field fertilisation doses in precision agriculture involve integrating agronomic and spatial components

The primary data sources for precision agriculture are derived from geomatics, including remote sensing, classification, and mapping. Geodesy, specifically in measurement works like GNSS positioning or laser scanning, also contributes significantly. Geomatics (in this case, remote sensing) proves particularly well-suited for applications in this field, thanks to its developed skills and competencies, as well as its sensitivity to the precision of measurements and the quality of resulting studies.

In the context of medium- and large-scale agriculture (areas of 100 ha and more), employing aircraft for agrotechnical procedures proves advantageous, as they can efficiently distribute fertilisers or plant protection products within a short timeframe. Aircraft also serve as effective carriers for remote sensing sensors capable of capturing spectral responses of soil and plants from a relatively low altitude. This capability ensures that the acquired images remain unaffected by disruptive factors such as cloud cover, fog, and, to some extent, rainfall or snowfall. In contrast, satellite remote sensing faces challenges, including low geometric resolution and the influence of atmospheric factors, which hinder the acquisition of current data. Unmanned aerial vehicles (UAVs) pose competition for aviation systems, primarily due to the miniaturisation of installed sensors and their ease of use, flexibility, and very high spatial resolution. However, UAVs currently grapple with limitations such as a relatively short range and operational difficulties stemming from adverse weather conditions like fog, moisture during rain, icing, frost, etc. (Lundby 2019, Rajawat & Gautam 2021, Giersch et al. 2022). These factors adversely affect both the control systems and the sensors themselves. Furthermore, the high resolution of UAVs can sometimes pose challenges in classifying image data due to the extensive diversity of recorded details. Nevertheless, this represents a burgeoning field in remote sensing, encompassing measurements of both plants and soil, as well as supporting other measurement systems by gauging factors such as weather conditions (Anil Kumar & Ambika 2020).

1.2. Motivation

The study's objective was to explore technological solutions designed to provide remote sensing support for agriculture from aerial platforms. Certain bands of electromagnetic radiation, known to exhibit a strong correlation with plant biomass while minimising the impact of shade and background/soil on natural analysis results, were investigated (De Petris et al. 2023). Vegetation indices (VI) emerged as effective tools for mapping, monitoring, and assessing crop changes, proving particularly suitable for agricultural applications. Successful research utilising VI can be conducted based on aerial imagery of the Earth's surface, necessitating image data acquisition with specific electromagnetic wavelengths.

A notable example of advancements in this field is the MultiSpectral Instrument (MSI) sensor, installed on the Sentinel-2 A/B satellites launched in 2015 as part of the ESA Copernicus space program (ESA 2014). The MSI is instrumental in obtaining image data for agricultural and forestry analyses. Noteworthy features of this sensor include the registration of reflected electromagnetic waves in three narrow "red edge" bands (with a geometric resolution of 20 m) and a relatively high time resolution of several days. While these satellite imaging parameters are well-suited for detecting most human-nature interactions (Chen J. et al. 2015) at the regional level, they exhibit limited suitability for analysing smaller fields with an area of up to several dozen hectares due to insufficient geometric resolution. Nonetheless, many authors highlight the specific spectral characteristics and the abundance of vegetation indices provided by the program based on the radiation bands recorded by MSI

(https://land.copernicus.eu/en/products/vegetation). VI find applications in biomass mapping in agriculture (Weiss et al. 2020) and forestry (Spadoni et al. 2020), as well as in assessing plant diseases (Marinelli et al. 2015) and conducting phenological assessments for the classification and monitoring of crops (Zhang et al. 2002).

As per agricultural literature, including reference (Xue & Su 2017, and others), widely-used vegetation indices derived from Sentinel-2 data include the Normalised Difference Vegetation Index (NDVI) and the Normalised Difference Red Edge Index (NDRE). NDVI, with roots tracing back to Rouse et al. (1974), who already 50 years ago proposed it for nature analyses, mainly due to the perceived advantages of the NIR band recorded along with the B, G and R bands by the satellites of that time. This index illustrates a high correlation with the Leaf Area Index (LAI), which so far confirms its usefulness in characterising the canopy and vigour of plants and crops (Sun et al. 2018) as a function of time and space. In agriculture, the NDRE index, relying on the NIR and RE channels, has proven effective in evaluating chlorophyll and nitrogen content in plants (Li et al. 2014). The G and R bands remain relevant, correlating with chlorophyll and other plant pigments, while broad NIR bands provide insights into leaf structure (Fernández-Manso A. et al. 2016).

The registration in the RE band refers to the rapid increase in the reflection coefficient of vegetation within the electromagnetic wave range from 680 nm to 750 nm. These frequencies correspond to two optical effects in plant tissue – significant chlorophyll absorption, leading to low reflectance near the red band (R), and substantial internal scattering of radiation by leaves, resulting in high reflectivity closer to the NIR wavelength. According to Xie et al. (2018), RE bands can markedly enhance the accuracy of biomass and yield estimates. In the Sentinel system, the 5th RE band of the MSI sensor (proximate to R) is linked to variations in chlorophyll content. In contrast, the 7th RE band (proximate to NIR) is associated with changes in leaf structure (Fernández-Manso A. et al. 2016). This approach is particularly apt for mapping diverse landscapes (Dong et al. 2019). Moreover, endeavours are underway to utilise MSI data for phenological phase estimation and phenometric extraction (Misra et al. 2020).

Widely utilised indices to monitor water in plants include NDVI and NDWI (Bannari et al. 2017, Prashar & Jones 2016). Publications underscore the significant utility of plant indices and enumerate their myriad applications. They also highlight their flaws or imperfections, prompting searching for new and improved solutions. In particular, concerning satellite systems, the issue of spatial resolution, which holds particular importance for smaller areas, is noted (Mulla 2013, Fernández-Quintanilla et al. 2019).

As a result, efforts are underway to identify remote sensing solutions suitable for detailed studies, relying on images captured from an aerial perspective (several hundred meters or more above ground level). More recently, there has been a growing trend in using UAVs, occasionally flown at altitudes rarely exceeding 100-150 m. Thanks to the progressive miniaturisation of sensors, unmanned vehicles can now carry multiple devices simultaneously, significantly enhancing their appeal. The literature showcases specific solutions employing various sensors in studies of tundra (Yang et al. 2020), savanna vegetation (Gaughan 2022), and various tasks within precision agriculture (Tsouros et al. 2019, Candiago et al. 2015, and others). Consequently, attempts are made to integrate traditional cameras with innovative remote sensing techniques such as spectroscopy, LiDAR, and thermal infrared (TIR) on UAVs (Yao et al. 2019). For instance, commercial RGB optical cameras, paired with multispectral cameras like Parrot Sequoia and MicaSense Red-Edge, have been employed in agricultural and grassland ecosystems to characterise vegetation composition under operational conditions (Fawcett et al. 2020). In (Zhu et al.2023), the multispectral sensor (G/R/RE/NIR channels), coupled with an RGB camera, is highlighted as standard equipment on popular DJI Mavic/Phantom Multispectral drones. Hyperspectral sensors are also integrated with a thermal camera (Zarco-Tejada et al. 2012) or LiDAR (Stankey et al. 2017), allowing the acquisition of specialised data for detecting water stress or monitoring other threats. Low-level UAV-based recording additionally enables the generation of a three-dimensional vegetation structure using the Structure-from-Motion (SfM) technique (Turner et al. 2012). Canopy Height Models (CHM) produced through this technique in forest ecosystems are comparable to the results of LiDAR measurements (Alonzo et al. 2018). Unfortunately, UAVs also exhibit the weaknesses above, significantly limiting their capabilities.

In contrast to drones, installing multiple remote sensing sensors on aircraft is not as widely adopted. In the 1970s, Goetz (1997) employed an airborne solution to replicate the Landsat MS sensor for measuring grassland surface temperature and biophysical variables. Using aerial recording with various sensors, Rowlands and Sarris (2007) explored traces of ancient buildings in Crete and achieved promising results. For agricultural land cover mapping, Vogels et al. (2017) utilised archival black and white aerial photos, achieving expected results through object-based classification (OBIA) and the Random Forest (RF) procedure. Information on similar solutions is challenging to find in contemporary literature.

As indicated by several bibliographic references, the lack of commercial solutions and the identified needs of farmers prompted the authors to develop and manufacture their own set of sensors mounted on aircraft. By emulating the radiometric characteristics of the MSI sensor but with significantly higher spatial resolution,

such a set had the potential to meticulously map plant features over relatively smaller areas. Additionally, it offered greater flexibility in temporal resolution compared to satellites. The designed solution emphasised obtaining data for calculating NDVI and NDRE indices. The anticipated benefits of directly measuring plant height were also considered, leading to the design of a set comprising cameras supplemented with a laser scanner (ALS). This set, installed on the aircraft and a system for stabilising and controlling all components from a single control module, ensures appropriate spatial and radiometric accuracy. It is flexible in terms of time and can cover areas (fields) ranging from several dozen to several hundred hectares at a time (Sieczkiewicz et al. 2024).

2. Methodology

2.1. Construction of a set of sensors for data recording

As highlighted in the introduction, the construction efforts aimed to simultaneously register several designated bands of electromagnetic radiation reflected from the soil and crops, coupled with altitude measurement. The efficient data acquisition should adhere to the block diagram illustrated in Figure 2. The activities delineated in the diagram represent a conceptual prototype of a multi-sensor aerial data acquisition system developed and manufactured by GISPRO S.A. under the name MultiSen-PL.

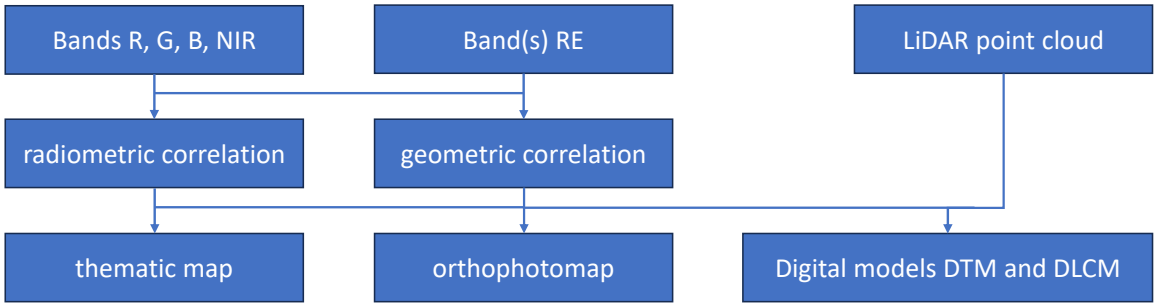

Fig. 2. Schematic diagram illustrating the acquisition of multi-sensor aerial data – MultiSen-PL (own study)

Given the initial experience with the MSI S-2 sensor and the absence of its aerial counterparts, the company opted to develop its own prototype set of sensors during the design phase. The concept involves utilising off-the-shelf hardware solutions, complemented by recording data in specific narrow electromagnetic bands (as depicted in the first line of the diagram). Following preliminary analyses, a hardware solution was chosen, incorporating a commercial airborne photogrammetric camera, a monochrome medium format camera equipped with an RE filter, and a commercial airborne scanner. The design challenge centred on integrating these sensors and the IMU and GNSS antennas into a cohesive set overseen by a unified control module.

A conceptual illustration of the comprehensive set of devices – encompassing sensors, INS, synchronisation, control, and power – installed on a single aircraft is presented in Figure 3.

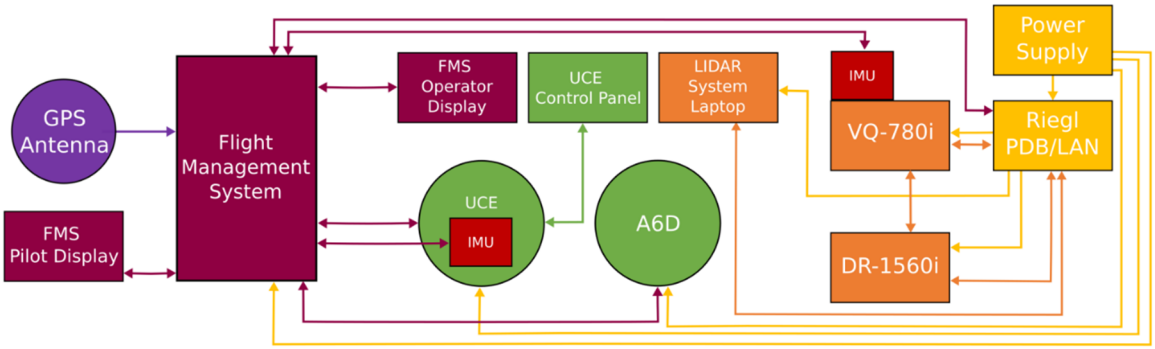

Fig. 3. Functional diagram detailing the installation, connection, and control of sensors comprising the on-board multispectral recording system MultiSen-PL (own work)

Imaging sensors are affixed to distinct stabilising beds, and their operation is synchronised with the recording system. The configuration of individual devices must prioritise flight safety, ease of operation, and accurate recording. Therefore, it hinges on factors such as the type of aircraft, its size, balance, and, from the photo-

grammetric perspective, the geometric alignment of all devices. Consequently, technological and design assumptions were developed concerning the spatial-temporal integration of spectral and spatial sensors and the parameterisation of their functional features. The transitional phase of the project involved installing the devices mentioned above on two planes and registering them via synchronous flight.

2.2. Principles of data processing

2.2.1. Geometric and radiometric correlation of remote sensing data

A data preprocessing stage (second row in Figure 2) is envisaged, acknowledging anticipated disparities between individual sensors in spatial and radiometric terms. This stage includes radiometric correlation of images – in practice, determining the ranges of DN values based on white balance – and geometric correlation, which involves adjusting (sharpening) lower-resolution images to a high-resolution reference image. Given the relatively undemanding spatial resolution required for agricultural classification purposes, an initial degradation of the original resolution of the reference image to the ground dimension of 10 × 10 cm was permitted.

The HCS (Hyper-spherical Color Sharpening) fusing method was selected to enhance image components with lower resolution, wherein only the intensity component (I) undergoes conversion as a direction vector in the hyperspherical colour space (Padwick et al. 2010). In HCS sharpening, the scale of this vector is altered based on the value of the panchromatic channel, either directly recorded or calculated from the B, G, and R bands, corresponding to a pixel in the spectral (colour) space. The HCS transformation is entirely universal and is independent of the number of channels and their individual resolutions. For an n-channel image, a general transformation of n-dimensional Cartesian space and n-dimensional spectral space can yield one intensity component and $n-1$ angles φ_i (Guo et al. 2017), following these formulas:

$$I^2 = \chi_1^2 + \chi_2^2 + \chi_3^2 + \cdots + \chi_n^2 \tag{1}$$

$$\begin{gathered} \varphi_1 = \tan^{-1}\left(\frac{\sqrt{\chi_n^2 + \chi_{n-1}^2 + \chi_{n-2}^2 + \cdots + \chi_2^2}}{\chi_1}\right) \\ \cdots \\ \varphi_{n-2} = \tan^{-1}\left(\frac{\sqrt{\chi_n^2 + \chi_{n-1}^2}}{\chi_{n-2}}\right) \\ \varphi_{n-1} = \tan^{-1}\left(\frac{\sqrt{\chi_n^2}}{\chi_{n-1}}\right) = \tan^{-1}\left(\frac{\chi_n}{\chi_{n-1}}\right) \end{gathered} \tag{2}$$

where χ_i represents the colour space component of the i-th spectral channel.

The following transformation is applied to compute the new value of the intensity component:

$$P'^2 = \frac{\sigma_0}{\sigma_1}(P^2 - \mu_1 + \sigma_1) + \mu_0 - \sigma_0 \tag{3}$$

$$I_{new} = \sqrt{P'^2} \tag{4}$$

where:
– P is the grey value in the Panchromatic image;
– μ_0 and σ_0 describe the mean and standard deviation of I^2;
– μ_1 and σ_1 describe the mean and standard deviation of P^2;

This process involves histogram matching. Based on these parameters, the angular values are converted into new values of the colour components:

$$\begin{gathered} \chi_1 = I_{new}\cos\varphi_1 \\ \chi_2 = I_{new}\sin\varphi_1\cos\varphi_2 \\ \cdots \\ \chi_{n-1} = I_{new}\sin\varphi_1\sin\varphi_2 \ldots \sin\varphi_{n-2}\cos\varphi_{n-1} \\ \chi_n = I_{new}\sin\varphi_1\sin\varphi_2 \ldots \sin\varphi_{n-2}\sin\varphi_{n-1} \end{gathered} \tag{5}$$

The approach described above Danoedoro & Gupita (2022) applied to data from the Landsat 8 satellite, and its modified form, HECS, was employed by Aiazzi et al. (2019) for data from the GeoEye satellite. It demonstrates its universal nature and suitability for sharpening images captured by various sensors recording in bands outside the visible range. Notably, Fletcher (2023), utilising WordView 3 farmland images, demonstrated that applying this method to convert 1.2 m spectral channels to 0.3 m resolution yielded some of the best results

among the 17 pansharpening methods tested. The slight blurring observed in satellite images sharpened using the HCS technique diminishes with increasing geometric resolution. Therefore, it was concluded that such blurring should not be significant, especially in the context of high-resolution aerial images, particularly concerning crop analyses.

2.2.2. Vegetation index maps and crop classification

For the development of thematic maps (third row in the diagram in Figure 2), the plan included preparing photo-interpretation keys based on the analysis of images processed using plant indices and field measurements of selected geometric features (and possibly spectral responses) obtained in situ at locations of the analysed crops reflected in the photos.

Consistent with the information on vegetation indices (VI), the methodological foundation involved creating maps based on the values of selected indicators, specifically the normalised differential vegetation index (NDVI), the corresponding NDRE index based on the RE channel, and optionally, the GNDVI and SAVI indices. These indices are defined using well-established mathematical rules (Xue & Su 2017):

- the NDVI index is calculated from the proportion: $\mathrm{NDVI} = \frac{\mathrm{NIR}-\mathrm{R}}{\mathrm{NIR}+\mathrm{R}}$, where: NIR and R mean the reflection of waves in the infrared and red bands, respectively;
- in the NDRE index, the R band is substituted with the RE ("edge") band, i.e., $\mathrm{NDRE} = \frac{\mathrm{NIR}-\mathrm{RE}}{\mathrm{NIR}+\mathrm{RE}}$;
- in the GNDVI index, the R band is substituted with the G band (green instead of red): $\mathrm{GNDVI} = \frac{\mathrm{NIR}-\mathrm{G}}{\mathrm{NIR}+\mathrm{G}}$;
- the last index under consideration, $\mathrm{SAVI} = \frac{\mathrm{NIR}-\mathrm{R}}{\mathrm{NIR}+\mathrm{R}+\mathrm{L}} \cdot (1+\mathrm{L})$ is based on the NDVI proportion. It incorporates the estimated L value that describes the ground cover with vegetation, ranging from $\mathrm{L} = 1$ for the land itself without plants to $\mathrm{L} = 0$ when the ground is not visible under the leaf canopy. This results in a value equal to NDVI under such conditions.

Additional cartographic products within the algorithm include an orthophoto map in natural colours, as a reference terrain image for the thematic maps and terrain models (DTM) and its cover (DLCM) developed utilising a registered LiDAR point cloud. Given the widespread utilisation of these products (Di Stefano et al. 2021, Koma et al. 2021), a detailed description has been omitted. To evaluate plant growth, their canopy height (CHM) is calculated as the difference between the numerical models, i.e., CHM = DLCM − DTM. This will serve as one of the features for assessing plant growth in the tested crops.

2.2.3. Test measurements for agricultural applications

In the context of targeted agricultural analyses, during the testing phase, a program was implemented to assess the health classes of corn crops based on the results of processing remote sensing data, including images and point clouds. The process involves assigning ranges of plant index values to one of several predefined quality classes (evaluating vigour, growth, and expected yields) of crop plants. The results obtained through this approach should assist agrotechnicians in deciding whether to apply necessary treatments in specific locations within a given field. The validation of a specific aviation laboratory, ultimately constituting the set of MultiSen-PL sensors, was planned to include an evaluation of the effectiveness of the classification method outlined above by comparing the results obtained with data from field measurements.

Figure 4 illustrates the flowchart outlining the adopted method for verifying the remote sensing assessment of crop plant quality based on field measurement data. The diagram comprises two blocks – the first pertaining to remote sensing analyses (located at the top of the figure) and the second encompassing the collected data from field measurements (at the bottom). Both sets of activities aim to evaluate the accuracy of plant classification using the MultiSen-1PL station.

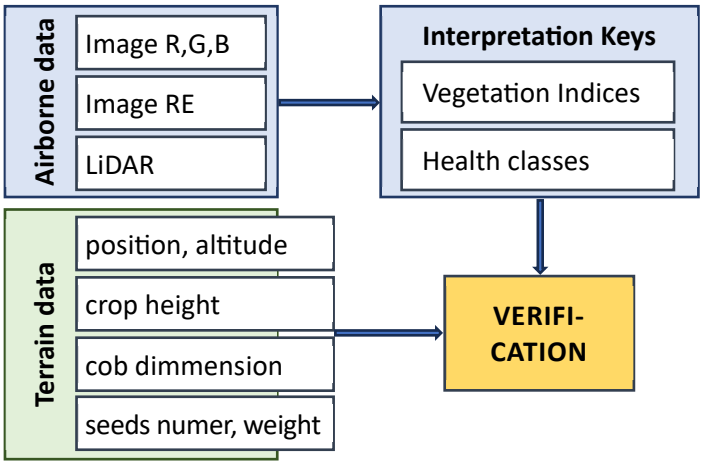

Fig. 4. Block diagram illustrating the method for field verification of quality analyses of crops (corn) determined based on remote sensing data from the MultiSen-1PL airborne station (own study)

Measurements were conducted at various stages of the development of the multispectral airborne set involving different equipment variants and diverse data acquisition methods. These tests culminated in creating and implementing the system, which was subsequently fine-tuned and certified. The set included test data on corn sowings throughout the growing season and just before harvest. Simultaneously, field measurements were conducted. The results of these efforts are summarised in the implementation section of this publication.

3. Implementation and Results

3.1. Hardware solution

To effectively utilise the presented set of sensors, it was imperative to ensure the simultaneous geometric projection of the recorded space, achievable through two methods: (a) sequential registration of image and height data using sensors on two (or several) air vehicles (2PL), or (b) employing a set of several sensors appropriately arranged on a single aircraft (1PL).

3.1.1. MultiSen-2PL intermediate solution

In developing this approach, initial tests were conducted by capturing test fields with two aircraft flying synchronously to ensure similar lighting conditions. The first plane was equipped with an UltraCAM Eagle photogrammetric camera, recording in B, G, R, and NIR channels; the second had a Hasselblad A6D medium resolution camera with an RE colour filter (radiation band 705-725 nm). Image synchronisation was achieved by independently conducting aerotriangulation and orthophoto processes in the same geometric space.

Cartographic preparation was carried out using the QGIS program (version 3.15). The data processed in this manner was utilised for calculating plant indices and formulating rules for the interpretation key for maise cultivation. It was assumed that key parameters would be adjusted based on field measurements for the target hardware solution.

The data obtained through this process facilitated the system refinement for a single aircraft, i.e., MultiSen-1PL.

3.1.2. MultiSen-1PL target solution

The MultiSen-1PL station comprises the two cameras mentioned above and the Riegl VQ780i scanner installed on the Vulcanair P68 TC Observer air platform. The aircraft is constructed in a classic configuration, measuring 9.45 m in length with a wingspan of 12 m. The wings are configured in a high-wing format with a rectangular outline. A schematic of the sensor arrangement in the aircraft is depicted in Figure 5.

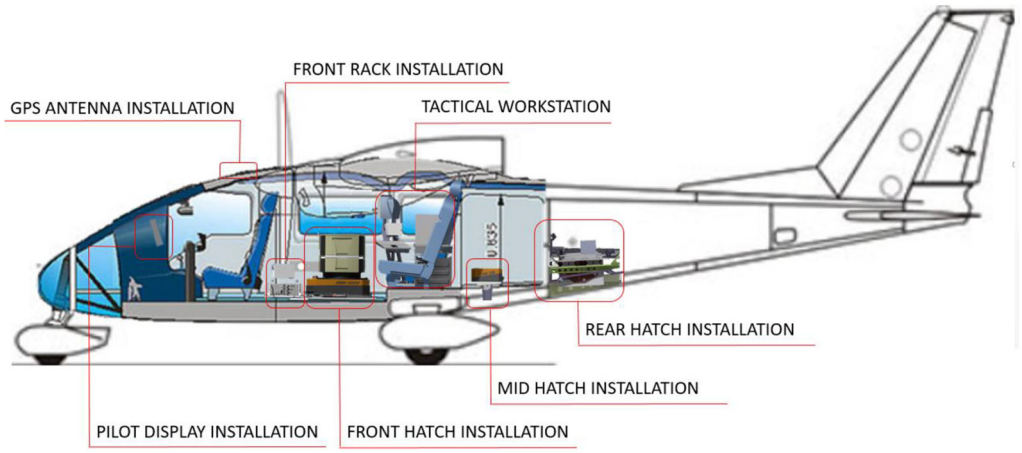

Fig. 5. Vulcanair P68 Observer aircraft indicating the placement of components comprising the MultiSen-1PL station

Following the adaptation of the aircraft for sensor installation, the platform, equipped with a set of remote sensing and navigation devices, underwent specialised tests and received necessary certification from an authorised entity to carry out modifications and approve changes following EASA (The European Authority for Aviation Safety) requirements. A series of measurements were conducted using the above set to demonstrate its utility for agricultural analyses, with a specific focus on developing and validating photo-interpretation keys established in earlier stages.

3.2. Test agricultural analyses

3.2.1. Processing and analysis of data from the MultiSen-PL station

The agricultural test analyses focused on selected maise fields in the village of Brzekiniec, situated in the Greater Poland Voivodeship, Chodzież County, Budzyń commune (Figure 6). Images of the test field, covering all five spectral channels and scanning, were acquired during runs on July 18-25, 2019, August 14, 2019, September 22, 2019, and July 18-19, 2020. PAN R+G+B+NIR images were recorded with an UltraCAM Eagle Mark3 camera, while the RE channel was captured with a Hasselblad A6D camera equipped with an optical filter. Simultaneously, all elements of external orientation were measured using the IGI Flight Management system with inertial units integrated with cameras.

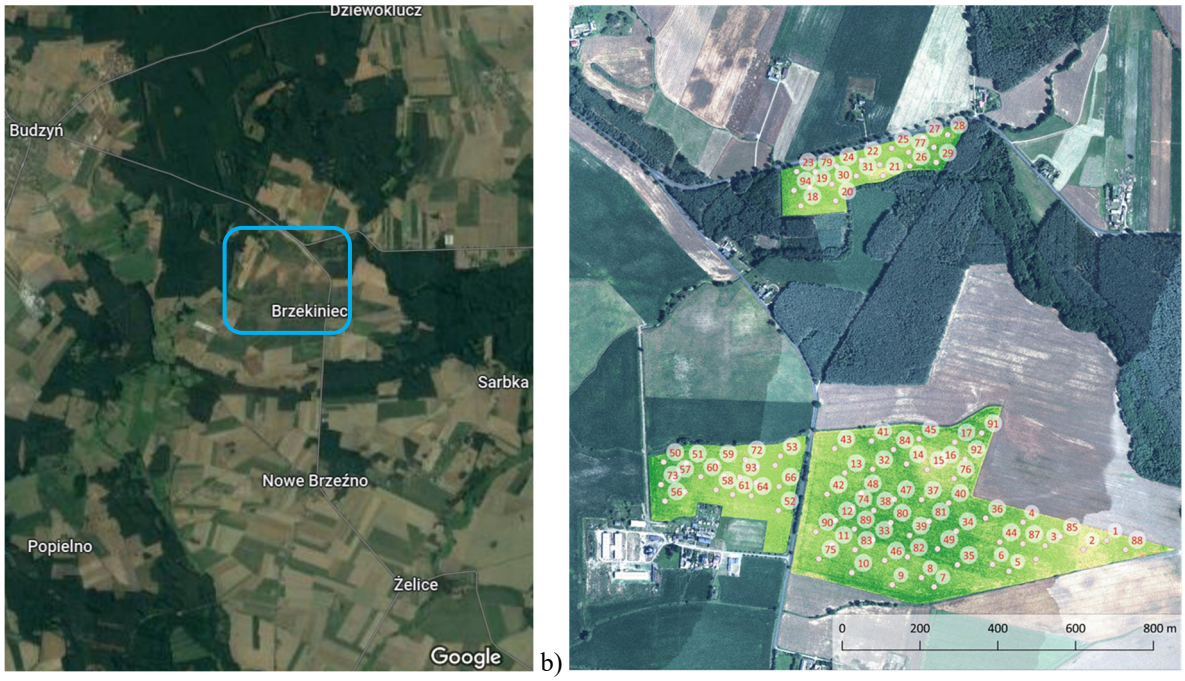

Fig. 6. Brzekiniec test area: a) location on Google map, b) orthophotomap with the location of measurement points (own work)

The RE data underwent geometric correction and were aligned with data from PAN channels. Subsequently, their resolution was enhanced through pansharpening using the HCS method. Radiometric alignment of the images was executed using three grey standards (18%) with dimensions of 70 × 70 cm distributed across the study area. The resulting 5-channel photos were the initial elements for creating orthophotomaps in selected three-channel compositions.

Spatial aerotriangulation was developed based on a field photogrammetric matrix measured in the field using GPS technology. The final alignment utilised the independent beam method, considering the Ebner model to calculate the camera auto-calibration parameters. The image data processed this way underwent automatic orthorectification using the bilinear method.

During the initial alignment of the ALS data, adjustments were made to the scanner calibration parameters. In the stage of mutual matching of the scans, orientation elements of individual scans were calculated, and the scanner calibration parameters were again corrected. The point cloud underwent initial automatic classification using Terrasolid software. The classification parameters were fine-tuned to assign individual cloud points to soil and vegetation classes accurately. A Digital Terrain Model and a Digital Land Cover Model were generated based on the classified point cloud. These models were compared for different point cloud densities ranging from 4 to 16 points/m^2 and across various campaigns.

3.2.2. Validation studies based on acquired remote sensing data

Aerial surveys were conducted on the mentioned dates to conduct agricultural analyses corresponding to different phases of plant growth. Through photogrammetric processing of images and scans, the analyst gained access to aligned B, G, R, NIR, and RE channels, as well as a point cloud. The tests were carried out each time for 100 measurement points located in the designated areas of the corn fields, as indicated in Figure 6b. Utilising the acquired image data, it became possible to calculate the GNDVI, NDVI, NDRE, and SAVI indices. Subsequently, concerning corn crops, groups of pixels corresponding to one of the five plant quality classes were isolated. Based on this, parameters for the photo interpretation of the keys mentioned above were established. These data underwent field verification to assess the consistency of the keys with the actual situation.

Field measurements of corn characteristics were conducted at the specified locations, following the guidelines outlined in Chapter 2. Validation tests and calibration of the interpretation key parameters were performed based on photos and measurements of plant characteristics. Figures 7a-c depict images of the southern field of the test area successively developed using the GNDVI, NDVI, and NDRE indices.

Data were collected at each specified location in five places – at the centroid and points spaced 0.5-1.0 m apart in the N, E, S, and W directions. The fieldwork documentation is depicted by selected photos in Figure 8, including corn cobs harvested at one of the measurement locations and measurements of canopy height in July 2019 and October 2019.

Differences in the established health classes were identified when comparing photo-interpretation keys derived from the analysis of aerial photos and ground measurements. A variance in the health class (i.e., assigning a point to a different class) was considered an error requiring correction in the keying algorithms.

As illustrated in Figure 9, a correlation table was generated by comparing field features and calculated vegetation indices. Field data collected in October, just before harvest, were compared with remote sensing data from July, covering the entire growing season. It allowed for assessing the effects of predicting target crop characteristics based on data obtained 3 months earlier. Numerical values in the range <0,1> enable an assessment of the extent to which features are correlated. This assessment guided the selection of features for further comparative analyses.

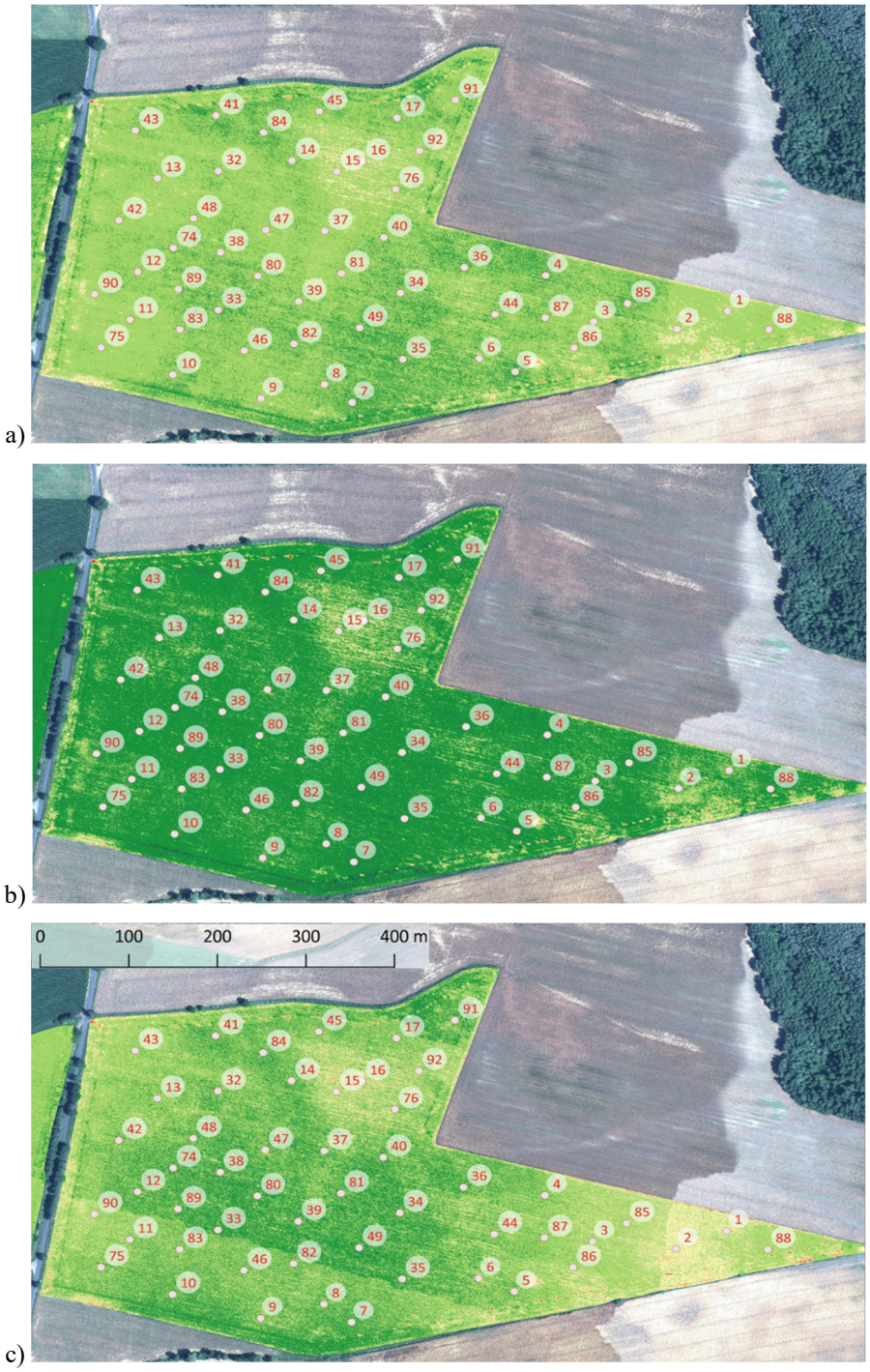

Fig. 7. Orthophotomap of the upper test area in Brzekiniec with measurement point locations overlaid on plant indices: (a) GNDVI, (b) NDVI, (c) NDRE. Captured in July 2019 (own study)

Fig. 8. Data from in-situ measurements: (a) variations in the size and quality of corn cobs within individual classes; (b) assessment of corn canopy height during the plant growth stage, (c) measurement of corn canopy height after the growing season (own study)

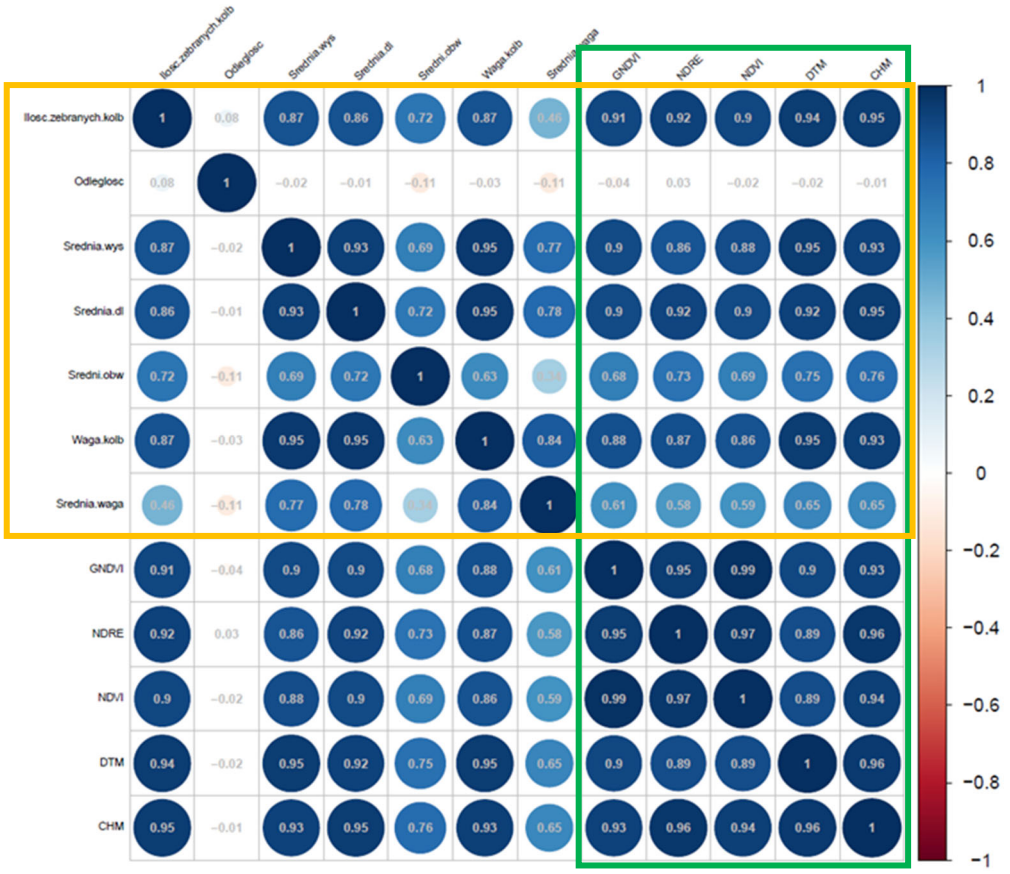

Fig. 9. Correlation table of measured characteristics in corn canopy test points: the gold frame encompasses correlations pertaining to data gathered in the field in October; the green frame pertains to indexes computed from remote sensing data in July, spanning the entire growing season; shared area – associations between indexes and field data (own study)

3.2.3. Analyses of the obtained results

In Figure 9, the results for field data are marked in gold, and the vegetation indices and the CHM height parameter results are marked in green. Concerning field measurements, there is a visible lack of correlation between the distance between plants and any other parameter, mainly since corn is usually planted at the same spacing (i.e. 70 cm). Meanwhile, a high correlation (i.e. 0.95) occurs between the weight (weight) of the cobs, the height of the plants and the length of the corn cobs; there is a slightly smaller correlation (0.94) between the height and length of the cobs. Therefore, for the final assessment, it was decided to select only one of these factors – height (CHM).

Concerning the acquired remote sensing data, the NDVI and GNDVI (0.99) and NDVI and NDRE (0.97) indices exhibit strong correlations, indicating that at the phenological stage during recording (i.e., in July), the plant response to light waves is essentially balanced. Notably, the correlation of plant indices with the CHM

parameter is intriguing, with the highest correlation found for the NDRE index (0.96) and slightly smaller correlations for NDVI (0.94) and GNDVI (0.93).

These observations prompted a detailed analysis in two categories:

1) The agreement of the heights obtained in the LiDAR measurement and their subsequent (final) field measurement.
2) The agreement of plant indexes with plant height at the end of the growing season.

Analysis of the consistency of height measurements in various stages of plant development

Seventeen well-documented locations were selected for measurement, with averaged results obtained from both measurement methods (1 × 1 m square around the adopted centroid). Based on the analysis, the chart shown in Figure 10 was created.

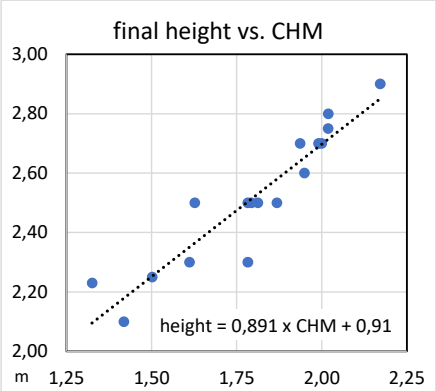

Fig. 10. Graph depicting the correlation between canopy height measured in July (CHM from LiDAR data) and field measurements in October. On average, plant heights increased by 0.91 m (own study)

The height relationship graph between various measurements in different growing seasons demonstrates very high consistency – the value of 0.91 in the trend line equation indicates that, on average, the plants increased by this amount between July and October 2019. The coefficient of 0.89, close to 1.0, implies an almost perfect scale of growth at all measurement sites. It should be noted, as evident in the maps of the test field, that this area is characterised by varying humidity, which significantly influences plant growth, introducing considerable variation in results (within 1 m). Nonetheless, in only three cases, the interpolated final heights differ from the actual heights by more than 0.1 m, while in the remaining cases, these differences are much smaller than 0.1 m.

Analysis of the compliance of plant indices with plant height at the end of the growing season

The subsequent analysis involved comparing three individual indices – GNDVI, NDVI, and NDRE (the SAVI index was omitted due to interpretation errors) – against the CHM parameter obtained in the same data registration process. They are presented in Figure 11.

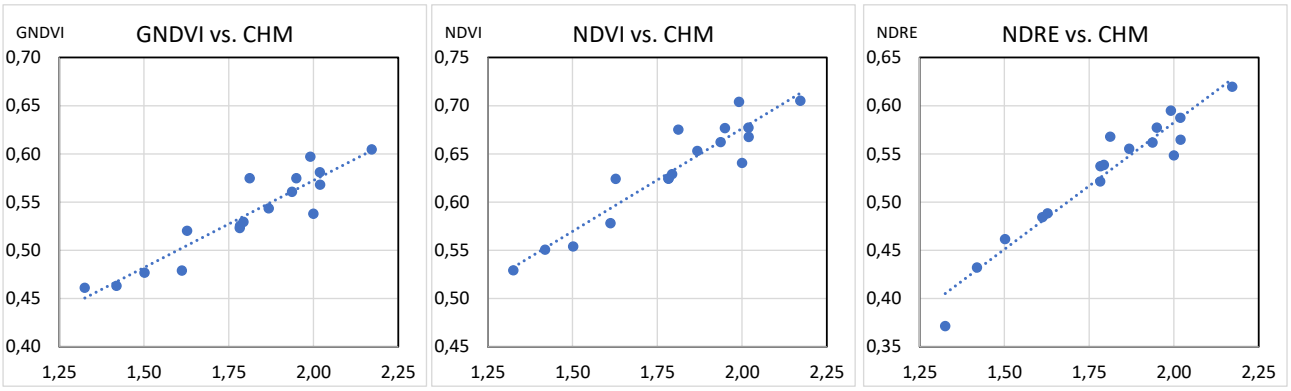

Fig. 11. Correlation results between index values at selected points in the test field and the LiDAR height measurement outcomes (own study)

The charts presented in Figure 11 indicate a relatively high agreement between the indices, which are 0.93, 0.94, and 0.96, respectively. It suggests that the NDRE index exhibits the strongest correlation with canopy height. The differences between the heights interpolated from the indices and the CHM measurement result are approximately 0.085 m for the GNDVI and NDVI indices and 0.065 m for the NDRE index. The correlations between the indices are 0.99 for the GNDVI and NDVI indices, 0.97 for NDVI and NDRE, and 0.95 for GNDVI and NDRE. Consequently, during the period of intense corn greening, there is practically no difference between GNDVI and NDVI, while the NDRE index slightly lags behind the others.

The last analysis is an experimental test to address whether arithmetic combinations between individual indices correlate with the plant growth parameter. The results of this test are presented in Figure 12.

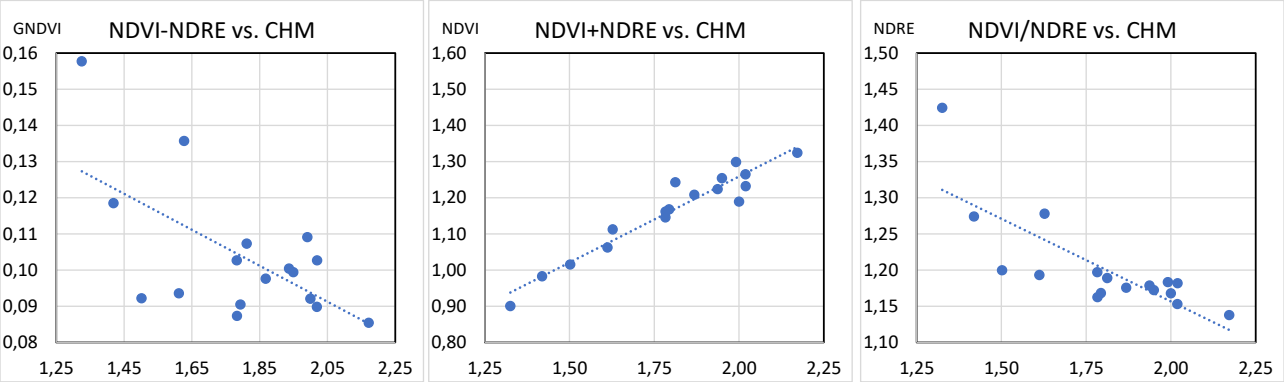

Fig. 12. Relationships between the difference, sum and quotient of the NDVI and NDRE indices and the canopy height parameter

Upon comparing the three charts in Figure 12, it is evident that the differences and ratios between the values of the NDVI and NDRE indices in the studied places exhibit poor correlation with the CHM heights. However, an intriguing result is demonstrated by the ratio of the sum (or the average) of NDVI + NDRE to the CHM. In this case, the correlation coefficient is 0.96, and the discrepancy between the predicted and measured canopy height is 0.065 m, similar to the NDRE index itself. The complete list of correlation coefficients between the values for individual indices and CHM and between combinations of indices and CHM, is presented in Table 1.

Table 1. Compilation of correlation parameters linking the values of examined vegetation indices and their combinations with the Canopy Height Model (CHM) growth parameter. These correlations were determined based on a sample collected during tests conducted with the MultiSen-1PL airborne remote sensing recording station in July 2019

	GNDVI		*NDVI*		*NDRE*		*CHM*
GNDVI	1						
NDVI	0,989		1				
NDRE	0,947		0,966		1		
CHM	0,929		0,939		0,963		1
	NDVI-NDRE		*NDVI+NDRE*		*NDVI/NDRE*		*CHM*
NDVI-NDRE	1						
NDVI+NDRE	0,584	(–)	1				
NDVI/NDRE	0,943	(+)	0,794	(–)	1		
CHM	0,624	(–)	**0,960**	(+)	0,790	(–)	1

The data presented in Table 1 concludes the series of small-scale analyses of the results from processing remote sensing data obtained with the MultiSen-PL aerial multi-sensor station. According to the authors, these results validate the construction efforts undertaken and serve as a starting point for further research on utilising this data in precision agriculture.

4. Discussion

The focus of the presented project was on constructing and implementing a multi-sensor aerial data recording system, its subsequent calibration and validation, and its application in agriculture and forestry. This text specifically addresses the selection of necessary remote sensing data, leading to a distinctive design solution and then subjecting it to agricultural tests, primarily concerning corn crops. In conceptualising the discussed

solution, it was assumed that the classification would rely on plant index maps using interpretation keys. Consequently, an in-depth analysis of the applications of specific indices (VI) and the subsequent selection of sensors were conducted to ensure appropriate data provision. Based on the bibliographic analysis, the NDVI, NDRE, and GNDVI and SAVI indices were chosen.

The designed analyses necessitate data recorded in the RE band, a frequency range not covered by the onboard sensors used thus far. Therefore, the MultiSen-PL aerial remote sensing station and the traditional B, G, R, and NIR channels ensure recording in this crucial band. The expanded set of acquired image data now includes LiDAR, providing height data enabling continuous assessment of plant growth.

Tests evaluating the growth and health of corn based on a broader spectral range reveal that such a sensor setup, equipped with appropriate computational mechanisms, allows for more accurate assessments. Consequently, it provides more effective and precise conclusions regarding the growth and vigour of crop plants over an extended growing period, compared to assessments solely based on NDVI.

One of the test objectives was to ascertain the extent to which the results from the analysis of remote sensing data obtained in this manner reflect the condition of plants at the end of the growing season. Positive outcomes in this regard would facilitate predicting the final effects of forgoing agrotechnical treatments, aiding in foreseeing future outcomes based on developmental models. This predictive potential was evaluated by examining the degree of alignment between the analysis of remote sensing data obtained during plant growth and the results of field measurements at the end of the growing season. The results exhibit a high degree of correlation (over 90%), providing a promising foundation for further research in this domain. Further tests covering a diverse range of crop species throughout the growing season are essential to affirm these conclusions and assess the broader efficacy of the discussed hardware solution. Such activities are planned for subsequent phases of system development.

5. Summary

Starting with the observed utility of nature analyses in the frequency range of electromagnetic waves on the border of the visible and near-infrared bands (referred to as RE – RedEdge), confirmed by the European Space Agency (ESA), it was deemed imperative that an airborne remote sensing set designed for agricultural diagnostics should include imaging in this band. To achieve this objective, a research project led to the development of a multi-sensor diagnostic station, MultiSen-1PL, housing various sensors on a single air vehicle. This station comprises a photogrammetric VNIR camera, a medium format monochrome camera optimised for recording in the RE band, and an ALS airborne scanner. This set, supplemented with stabilisation beds, INS, and a common control panel, is capable of synchronous image registration in five spectral channels in combination with a point cloud, ensuring field spatial resolution of no less than 10 × 10 cm.

Following the installation, calibration, and validation of the set mentioned above, trial tests were conducted to assess the condition of the corn crop on a selected test field, characterised by a relatively large diversity of plant growth. A classification system divided into five quality classes based on plant index maps was used to assess the quality of the crop. The NDRE indicator, which considers imaging in the RE channel, was used as a competitor to the classic indicators such as NDVI, GNDVI, and SAVI. The tests revealed that, during the plant growth period, the assessment based on the NDRE index yielded comparable or slightly better results than the others. Noteworthy findings were also obtained by assessing the target height of plants at the end of the growing season based on images from July. Classification using the RE channel demonstrated the highest correlation with the growth parameter. The obtained results are an incentive to undertake further research on a larger scale, which, in the authors' opinion, should result in a reliable method for assessing crop quality based on the analysis of remote sensing data from the MultiSen-1PL diagnostic station presented here.

The research was carried out under the grant of the National Center for Research and Development POIR.01.01.01-00-1071/17-00: "Research and development work on the prototype technology of a multisensory aerial diagnostic station, enabling large-scale inventory and parameterisation of vegetation" implemented in 2018-2020.

References

Aiazzi, B., Alparone, L., Arienzo, A., Garzelli, A., Lolli, S. (2019). Fast multispectral pansharpening based on a hyperellipsoidal color space, *Proc. SPIE 11155, Image and Signal Processing for Remote Sensing XXV*. *1115507*. https://doi.org/10.1117/12.2533481

Alonzo, M., Andersen, H.-E., Morton, D., Cook, B. (2018). Quantifying Boreal Forest Structure and Composition Using UAV Structure from Motion. *Forests. 9*(3), 119. https://doi.org/10.3390/f9030119

Bannari, A., Mohamed, A.M.A., El-Battay, A. (2017). Water stress detection as an indicator of red palm weevil attack using WorldView-3 data. In: *Proceedings of the 2017 IEEE International Geoscience and Remote Sensing Symposium (IGARSS)*, FortWorth, TX, USA, July 23 2017, 4000-4003. https://doi.org/10.1109/IGARSS.2018.8518687

Bogue, R. (2017). Sensors key to advances in precision agriculture. *Sensor Review*. *37*(1), 1-6. https://doi.org/10.1108/SR-10-2016-0215

Camilli, A., Cugnasca, C.E., Saraiva, A.M., Hirakawa, A.R., Corrêa, P.L.P. (2007). From wireless sensors to field mapping: Anatomy of an application for precision agriculture. *Computers and Electronics in Agriculture*. *58*(1), 25-36. https://doi.org/10.1016/j.compag.2007.01.019

Candiago, S., Remondino, F., De Giglio, M., Dubbini, M., Gattelli, M. (2015). Evaluating Multispectral Images and Vegetation Indices for Precision Farming Applications from UAV Images. *Remote Sensing* 7, 4026-4047. https://doi.org/10.3390/rs70404026

Chen, J., Chen, J., Liao, A., Cao, X., Chen, L., Chen, X., He, C., Han, G., Peng, S., Lu, M., et al. (2015). Global land cover mapping at 30 m resolution: A POK-based operational approach. *ISPRS J. Photogramm. Remote Sens. 103*, 7-27. https://doi.org/10.1016/j.isprsjprs.2014.09.002

Danoedoro, P., Gupita, D.D. (2022). Combining Pan-Sharpening and Forest Cover Density Transformation Methods for Vegetation Mapping using Landsat-8 Satellite Imagery. *International Journal on Advanced Science Engineering and Information Technology*, *12*, 881-891. https://doi.org/10.18517/ijaseit.12.3.12514.

De Petris, S., Sarvia, F., Borgogno-Mondino, E. (2023). Uncertainty assessment of Sentinel-2-retrieved vegetation spectral indices over Europe. *European journal of remote sensing*, 1-14. https://doi.org/10.1080/22797254.2023.2267169

Diedrichs, A.L., Tabacchi, G., Grunwaldt, G., Pecchia, M., Mercado, G., Antivilo, F.G. (2014). Low-Power Wireless Sensor Network for Frost Monitoring. In: *Agriculture Research. IEEE Biennial Congress of Argentina*, 11-13 June 2014. https://doi.org/10.1109/ARGENCON.2014.6868546

Di Stefano, F., Chiappini, S., Gorreja, A., Balestra, M., Pierdicca R. (2021). Mobile 3D scan LiDAR: a literature review. *Geomatics, Natural Hazards and Risk*. *12*(1). https://doi.org/10.1080/19475705.2021.1964617

Dong, T., Liu, J., Shang, J., Qian, B., Ma, B., Kovacs, J.M., Walters, D., Jiao, X., Geng, X., Shi, Y. (2019). Assessment of red-edge vegetation indices for crop leaf area index estimation. *Remote Sens. Environ. 222*, 133-143. https://doi.org/10.1016/j.rse.2018.12.032

ESA. Sentinel-2 Missions-Sentinel Online, ESA: Paris, France, 2014. Pobrano z https://sentinels.copernicus.eu/web/sentinel/missions/sentinel-2 (1.11.2023)

Fawcett, D., Panigada, C., Tagliabue, G., Boschetti, M., Celesti, M., Evdokimov, A., Biriukova, K., Colombo, R., Miglietta, F., Rascher, U., et al. (2020). Multi-Scale Evaluation of Drone-Based Multispectral Surface Reflectance and Vegetation Indices in Operational Conditions. *Remote Sensing*, *12*, 514. https://doi.org/10.3390/rs12030514

Fernández-Manso, A., Fernández-Manso, O., Quintano, C. (2016). SENTINEL-2A red-edge spectral indices suitability for discriminating burn severity. *International Journal of Applied Earth Observation and Geoinformation*, *50*, 170-175. https://doi.org/10.1016/j.jag.2016.03.005

Fernández-Quintanilla, C., Peña, J.M., Andújar, D., Dorado, J., Ribeiro, A., López-Granados, F. (2018). Is the current state of the art of weed monitoring suitable for site-specific weed management in arable crops? *Weed Research*, *58*, 259-272. https://doi.org/10.1111/wre.12307

Fisher, D.K., Kebede, H. (2010). A low-cost microcontroller-based system to monitor crop temperature and water status. *Computers and Electronics in Agriculture*, *74*(1), 168-173. https://doi.org/10.1016/j.compag.2010.07.006

Fletcher R.S. Comparing Pan-Sharpening Algorithms to Access an Agriculture Area: A Mississippi Case Study. (2023). *Agricultural Sciences*, *14*(9), 1206-1221. https://doi.org/10.4236/as.2023.149081

Gaughan, A.E., Kolarik, N.E., Stevens, F.R., Pricope, N.G., Cassidy, L., Salerno, J., Bailey, K.M., Drake, M., Woodward, K., Hartter, J. (2022). Using Very-High-Resolution Multispectral Classification to Estimate Savanna Fractional Vegetation Components. *Remote Sensing*, *14*, 551. https://doi.org/10.3390/rs14030551

Giersch, S., Guernaoui, O.E., Raasch, S., Sauer, M., Palomar, M. (2022). Atmospheric flow simulation strategies to assess turbulent wind conditions for safe drone operations in urban environments. *Journal of Wind Engineering and Industrial Aerodynamics*, *229*, 105136. https://doi.org/10.1016/j.jweia.2022.105136

Goetz, S.J. (1997). Multi-sensor analysis of NDVI, surface temperature and biophysical variables at a mixed grassland site. *International Journal of Remote Sensing*. *18*(1), 71-94. https://doi.org/10.1080/014311697219286

Guo, Q., Ehlers, M., Wang, Q., Pohl, Ch., Hornberg, S., Li, A. (2017). Ehlers pan-sharpening performance enhancement using HCS transform for n-band data sets. *International Journal of Remote Sensing*, *38*(17), 4974-5002. https://doi.org/10.1080/01431161.2017.1320448

Koma, Z., Zlinszky, A., Bekő, L., Burai, P., Seijmonsbergen, A.C., Kissling, W.D. (2021). Quantifying 3D vegetation structure in wetlands using differently measured airborne laser scanning data. *Ecological Indicators*, *127*, 107752. https://doi.org/10.1016/j.ecolind.2021.107752

Kumar, D., Ambika, R. (2020). Drone integrated weather sensors for agriculture purpose. *Int. Journal of Electrical Engineering and Technology (IJEET)*, *11*(5), 83-90. https://doi.org/10.34218/IJEET.11.5.2020.009

Li, F., Miao, Y., Feng, G., Yuan, F., Yue, S., Gao, X., Liu, Y., Liu, B., Ustin, S.L., Chen, X. (2014). Improving estimation of summer maise nitrogen status with red edge-based spectral vegetation indices. *Field Crops Research*, *157*, 111-123. https://doi.org/10.1016/j.fcr. 2013.12.018

Lundby, T., Christiansen, M.P., Jensen K. (2019). *Towards a weather analysis software framework to improve UAS operational safety*. 2019 International Conference on Unmanned Aircraft Systems, ICUAS, IEEE, Atlanta, GA, United States. 1372-1380. https://doi.org/10.1109/ICUAS.2019.8798271

Martinelli, F., Scalenghe, R., Davino, S., Panno, S., Scuderi, G., Ruisi, P., Villa, P., Stroppiana, D., Boschetti, M., Goulart, L.R. (2015). Advanced methods of plant disease detection. *A Review Agronomy for Sustainable Development*, *35*(1), 1-25. https://doi.org/10. 1007/s13593-014-0246-1

Misra, G., Cawkwell, F., Wingler, A. (2020). Status of Phenological Research Using Sentinel-2 Data: *A Review. Remote Sensing*, *12*(17), 2760. https://doi.org/10.3390/rs12172760

Mogili, UM R., Deepak, B.B.V.L. (2018). Review on Application of Drone Systems in Precision Agriculture. *Procedia Computer Science*, *133*, 502-509. https://doi.org/10.1016/j.procs.2018.07.063

Mulla, D.J. (2013). Twenty-five years of remote sensing in precision agriculture: Key advances and remaining knowledge gaps. *Biosyst. Eng.*, *114*, 358-371. https://doi.org/10.1016/j.biosystemseng.2012.08.009

Padwick, C., Deskevich, M., Pacifici, F., Smallwood, S. (2010). WorldView-2 pan-sharpening. In *Proceedings of the ASPRS 2010 Annual Conference, San Diego, CA, USA*, April 27, 2010, 1-14.

Prashar, A., Jones, H.G. (2016). Assessing drought responses using thermal infrared imaging. In: *Environmental Responses in Plants*, Humana Press: New York, NY, USA. 209-219. https://doi.org/10.1007/978-1-4939-3356-3_17

Radočaj, D., Jurišić, M., Gašparović, M. (2022). The Role of Remote Sensing Data and Methods in a Modern Approach to Fertilisation in Precision Agriculture. *Remote Sensing*, *14*, 778. https://doi.org/10.3390/rs14030778

Rajawat, M., Gautam, S. (2021). Weather conditions and its effects on UAS. *Int. Research Journal of Modernization in Engineering Technology and Science*, *12*, 255-261. Retrieved from: https://www.irjmets.com/uploadedfiles/paper/volume_3/issue_12 (1.11.2023)

Rose, D.C., and Chilvers, J. (2018). Agriculture 4.0: Broadening Responsible Innovation in an Era of Smart Farming. *Front. Sustain. Food Syst.*, *2*, 87. https://doi.org/10.3389/fsufs.2018.00087

Rouse, J.W., Haas, R.H., Schell, J.A., Deering, D.W., Harlan, J.C. (1974). Monitoring the vernal advancement and retrogradation (green wave effect) of natural vegetation. *NASA/GSFC Type III Final Report, Greenbelt, Md*, 1974, 371. Retrieved from: https://ntrs.nasa.gov/api/citations/19740022555 (1.11.2023)

Rowlands, A., Sarris A. (2007). Detection of exposed and subsurface archaeological remains using multi-sensor remote sensing. *Journal of Archaeological Science*, *34*(5), 795-803. https://doi.org/10.1016/j.jas.2006.06.018

Sankey, T., Donager, J., McVay, J., Sankey, J.B. (2017). UAV lidar and hyperspectral fusion for forest monitoring in the southwestern USA. *Remote Sens. Environ.*, *195*, 30-43. https://doi.org/10.1016/j.rse.2017.04.007

Sieczkiewicz, M., Jedynak, Ł, Wyczałek, I., Strzeliński, P., Wyczałek-Jagiełło, M. Wielosensorowy lotniczy system teledetekcyjny MultiSen-1PL na potrzeby precyzyjnego rolnictwa i leśnictwa. (2024). Multi-sensor airborne remote sensing system MultiSen-1PL for precision agriculture and forestry. *Przegląd Geodezyjny*. (in Polish) <in the review>

Spadoni, G.L., Cavalli, A., Congedo, L., Munafò, M. (2020). Analysis of Normalised Difference Vegetation Index (NDVI) multi-temporal series for the production of forest cartography. *Remote Sensing Applications: Society and Environment*, *20*, 100419. https://doi.org/10.1016/j.rsase.2020.100419

Sun, Y., Ren, H., Zhang, T., Zhang, C., Qin, Q. (2018). Crop leaf area index retrieval based on inverted difference vegetation index and NDVI. *IEEE Geosci. Remote*. *15*(11), 1662-1666. https://doi.org/10.1109/LGRS.2018.2856765

Tayari, E., Jamshid, A.R., Goodarzi, H.R. (2015). Role of GPS and GIS in precision agriculture. *Journal of Scientific Research and Development*, *2*(3), 157-162. Retrieved from: www.jsrad.org (1.11.2023)

Tian-en C., Li-ping C., Yunbin G., Yanji, W. (2009). Spatial Decision Support System for Precision Farming Based on GIS Web Service, *2009 International Forum on Information Technology and Applications*, Chengdu, China, 372-376, https://doi.org/10.1109/IFITA.2009.550

Triantafyllou, A., Sarigiannidis, P., Bibi, S. (2019). Precision Agriculture: A Remote Sensing Monitoring System Architecture. *Information*, *10*, 348. https://doi.org/10.3390/info10110348

Tsouros, D.C., Bibi, S., Sarigiannidis, P.G. (2019). A Review on UAV-Based Applications for Precision Agriculture. *Information*, *10*, 349. https://doi.org/10.3390/info10110349

Turner, D., Lucieer, A., Watson, C. (2012). An Automated Technique for Generating Georectified Mosaics from Ultra-High Resolution Unmanned Aerial Vehicle (UAV) Imagery, Based on Structure from Motion (SfM) Point Clouds. *Remote Sensing (Basel)*, *4*, 1392-1410. https://doi.org/10.3390/rs4051392

Vogels, M.F.A., de Jong, S.M., Sterk, G., Addink, E.A. (2017). Agricultural cropland mapping using black-and-white aerial photography, Object-Based Image Analysis and Random Forests. *International Journal of Applied Earth Observation and Geoinformation*, *54*, 114-123. https://doi.org/10.1016/j.jag.2016.09.003

Weiss, M., Jacob, F., & Duveiller, G. (2020). Remote sensing for agricultural applications: A meta-review. *Remote Sensing of Environment*, 236, 111402. https://doi.org/10.1016/j.rse.2019.111402

Xie, Q., Dash, J., Huang,W., Peng, D., Qin, Q., Mortimer, H., Casa, R., Pignatti, S., Laneve, G., Pascucci, S., et al. (2018). Vegetation indices combining the red and red-edge spectral information for leaf area index retrieval. *IEEE J. Sel. Top. Appl. Earth Obs. Remote Sens.*, *11*, 1482-1493. https://doi.org/10.1109/JSTARS.2018.2813281

Xue, J., Su, B. (2017). Significant remote sensing vegetation indices: A review of developments and applications. *Journal of Sensors*, 1-17. https://doi.org/10.1155/ 2017/1353691

Yang, D., Meng, R., Morrison, B.D., McMahon, A., Hantson, W., Hayes, D.J., Breen, A.L., Salmon, V.G., Serbin, S.P. (2020). A Multi-Sensor Unoccupied Aerial System Improves Characterisation of Vegetation Composition and Canopy Properties in the Arctic Tundra. *Remote Sens.*, *12*, 2638. https://doi.org/10.3390/rs12162638

Yao, H., Qin, R., Chen, X. (2019). Unmanned Aerial Vehicle for Remote Sensing Applications – A Review. *Remote Sensing (Basel)*. *11*(12), 1443. https://doi.org/10.3390/rs11121443

Zarco-Tejada, P.J., González-Dugo, V., Berni, J.A.J. (2012). Fluorescence, temperature and narrow-band indices acquired from a UAV platform for water stress detection using a micro-hyperspectral imager and a thermal camera. *Remote Sens. Environ. 117*, 322-337. https://doi.org/10.1016/j.rse.2011.10.007

Zhang, X., Friedl, M.A., Schaaf, C.B., Strahler, A.H., Hodges, J.C.F., Gao, F., Reed, B.C., Huete, A. (2002) Monitoring vegetation phenology using MODIS. *Remote Sensing of Environ*., *84*(3), 471-475. https://doi.org/10.1016/S0034-4257(02)00135-9

Zhu, Y., Liu, J., Tao, X., Su, X., Li, W., Zha, H., Wu, W., Li, X. (2023). A Three-Dimensional Conceptual Model for Estimating the Above-Ground Biomass of Winter Wheat Using Digital and Multispectral Unmanned Aerial Vehicle Images at Various Growth Stages. *Remote Sens.*, *15*, 3332. https://doi.org/10.3390/rs15133332